Observations of iodine oxide in the Indian Ocean marine boundary layer: A transect from the tropics to the high latitudes

Anoop S. Mahajan[a],[*], Liselotte Tinel[b], Shrivardhan Hulswar[c], Carlos A. Cuevas[d], Shanshan Wang[d], Sachin Ghude[a], Ravidas K. Naik[e], Rajani K. Mishra[e], P. Sabu[e], Amit Sarkar[e], N. Anilkumar[e], Alfonso Saiz Lopez[d]

[a] Centre for Climate Change Research, Indian Institute of Tropical Meteorology, Pune, India
[b] Wolfson Atmospheric Chemistry Laboratories, Department of Chemistry, University of York, YO10 5DD, UK
[c] Department of Marine Sciences, Goa University, Goa, India
[d] Department of Atmospheric Chemistry and Climate, Institute of Physical Chemistry Rocasolano, CSIC, Madrid, Spain
[e] National Centre for Antarctic and Ocean Research, Goa, India

HIGHLIGHTS

- Latitudinal transect for atmospheric iodine species in Indian and Southern Ocean.
- Model discrepancy suggests iodine chemistry is poorly understood in the SO.
- Inorganic HOI and I_2 fluxes are poor proxies for predicting IO over the SO.
- Chlorophyll *a* correlates better indicating a missing biogenic source in that region.

ARTICLE INFO

ABSTRACT

Observations of iodine oxide (IO) were made in the Indian Ocean and the Southern Ocean marine boundary layer (MBL) during the 8th Indian Southern Ocean Expedition. IO was observed almost ubiquitously in the open ocean with larger mixing ratios south of the Polar Front (PF). Contrary to previous reports, IO was not positively correlated to sea surface temperature (SST)/salinity, or negatively to chlorophyll *a*. Over the whole expedition, SST showed a weak negative correlation with respect to IO while chl *a* was positively correlated. North of the PF, chl *a* showed a strong positive correlation with IO. The computed HOI and I_2 fluxes do not show any significant correlation with atmospheric IO. Simulations with the global CAM-Chem model show a reasonably good agreement with observations north of the PF but the model fails to reproduce the elevated IO south of the PF indicating that the current emission parametrizations are not sufficient to explain iodine chemistry in the Southern Indian Ocean.

1. Introduction

Reactive iodine compounds play a critical role in regulating the chemistry of the troposphere due to their catalytic role in the depletion of ozone, changing the oxidizing capacity and formation of new particles (Saiz-Lopez and von Glasow, 2012). Initially both bromine and iodine were thought to affect atmospheric chemistry mainly in the polar environment where elevated concentrations (> 10 parts per trillion by volume, pptv, equivalent to picomole mole^{-1}) were observed, especially during the spring time e.g., (Frieß et al., 2001; Hausmann and Platt, 1994; McConnell et al., 1992; Saiz-Lopez et al., 2007b). However, observations over the last decade have shown that halogen oxides can play an important role even in the marine boundary layer (MBL) outside the polar environment (Alicke et al., 1999; Coburn et al., 2011; Dix et al., 2013; Großmann et al., 2013; Leser et al., 2003; Mahajan et al., 2012, 2010; Martin et al., 2009; Prados-Roman et al., 2015; Read et al., 2008; Saiz-Lopez and Plane, 2004; Wang et al., 2014).

Outside the polar environment and away from large coastal macro algae emissions, the first observations of IO were made at Cape Grim, Tasmania and later at the Canary Islands, showing a peak of 2.2 pptv and 4 pptv respectively (Allan et al., 2000). More recent observations at Cape Verde showed year round presence of IO at about 1.5 pptv, with

---

little annual variability (Mahajan et al., 2010; Read et al., 2008). Since these island based campaigns, ship based studies have confirmed the presence of IO in the remote MBL (Commane et al., 2011; Großmann et al., 2013; Mahajan et al., 2012; Prados-Roman et al., 2015), with IO mixing ratios typically around 1 pptv.

According to model estimates, there should be a large geographical variation in the IO mixing ratios in the Indian Ocean, with higher concentrations observed in the tropics and extra tropics (Prados-Roman et al., 2015; Saiz-Lopez et al., 2012; Sherwen et al., 2016b). The gradient is mainly driven by the emission strength of inorganic source gases, which peak in the tropics. The peak surface levels of IO differ according to the model used, with a peak ranging from 0.5 to 1 pptv (Prados-Roman et al., 2015; Sherwen et al., 2016b) close to the Indian subcontinent or the equator and < 0.2 pptv in the Southern Ocean.

Despite the few studies mentioned above, observations of IO are rare in the remote MBL and further measurements are necessary to validate model results. Aside from a cruise in the Southern Indian Ocean (Prados-Roman et al., 2015) and ground based observations at Maldives (Oetjen, 2009), there are no other reported observations of IO in this region. Here, we present observations of IO in the Indian Ocean, on a cruise from India to the Southern Ocean. The cruise enabled the study of a latitudinal transect from the Indian subcontinent to the Southern Ocean. Observations of IO and ozone are then compared to model simulations and their distribution is discussed in detail.

2. Observation and methodology

The study was conducted on board the oceanographic research vessel Sagar Nidhi as a part of the 8th Indian Southern Ocean Expedition (8th-ISOE) in January–February 2015. The expedition started at Chennai, India on 7th January 2015 and after observations in the Southern Ocean, the campaign finished in Mauritius on 22nd February 2015. Fig. 1 shows the track of the ship and the 5 day back trajectories arriving at noon every day of the cruise calculated using the HYbrid Single-Particle Lagrangian Integrated Trajectory (HYSPLIT) model (Draxler and Rolph, 2003).

2.1. Atmospheric observations

Surface ozone was monitored using an US-EPA approved photometric UV analyser (Ecotech EC9810B). Zero and span calibration of the O_3 analyser was done every other day using an inbuilt O_3 calibrator

and with gas standards before and after the expedition, which showed a ~5% drift. The O_3 analyser was placed at the same place as the indoor unit of the multi axis differential optical absorption spectroscopy (MAX-DOAS), with an inlet close to the outdoor unit (~2 m inlet gas line).

A MAX-DOAS (Hönninger et al., 2003; Plane and Saiz-Lopez, 2006; Platt and Stutz, 2008; Wagner et al., 2004) instrument (EnviMes) was set up on the second level of the ship, pointing towards the front with a clear line of sight to the horizon. The two part instrument is made up of an indoor unit, housing two spectrometers with a spectral resolution of 0.7 nm (UV: 301.20–463.69 and VIS: 443.54–584.19), which is connected to an outdoor unit, containing a scanning telescope. The outdoor unit was mounted on a mechanical gimbal table. This setup reduced the oscillations caused by the pitch and roll of the ship to within ± 2°. Additionally, the scanner incorporates a high sensitivity (± 0.01°) fast response (0.1 s) inclinometer and actively corrects the elevation angle. The true elevation angle was also logged and angles within a range of 0.2° were used for analysis. Spectra were recorded at discrete elevation angles (1°, 2°, 3°, 5°, 7°, 10°, 20°, and 90°) and were analysed using the QDOAS software for the retrieval of IO (415–440 nm spectral window) and O_4 (350–386 nm) differential slant column densities (DSCDs) (Fayt and Van Roozendael, 2013). The cross-sections used for IO retrieval in the 415–440 nm spectral window were: IO (Gómez Martín et al., 2005), NO_2 220 K and 298 K (Vandaele et al., 1997), H_2O (Rothman et al., 2013), O_4 (Greenblatt et al., 1990), O_3 (Bogumil et al., 2003), liquid water (Pope and Fry, 1997), a ring spectrum (Chance and Spurr, 1997), a second ring spectrum following (Wagner et al., 2009) and the 3rd order polynomial. The residual RMS in the IO region was between 1.5×10^{-4} to 5×10^{-4}, resulting in 2σ IO differential slant column densities (DSCDs) detection limits of 8.5×10^{12} to 2.8×10^{13} molecules cm^{-2}. For O_4, the spectral range was 350–386 nm with BrO (Wilmouth et al., 1999), and HCHO (Meller and Moortgat, 2000), in addition to O_3 223 K and 243K, NO_2 220 K and 298 K, O_4 and two ring spectra included with a 3rd degree polynomial. An example of the fits is shown in Fig. 2. The resultant DSCDs for O_4 and IO are shown in Fig. 3. Surface mixing ratios were calculated from the MAX-DOAS DSCDs using the O_4 slant columns retrieved during the study by the "O_4 method" (Mahajan et al., 2012; Prados-Roman et al., 2015; Sinreich et al., 2010; Wagner et al., 2004). To obtain the effective light path length, the O_4 DSCDs at the lower elevation angles (1º-3º) were divided by the assumed O_4 mean concentration from the surface to 200 m above sea level. The average scattering height was based on the average last scatter altitude calculated with NIMO fully spherical Monte Carlo
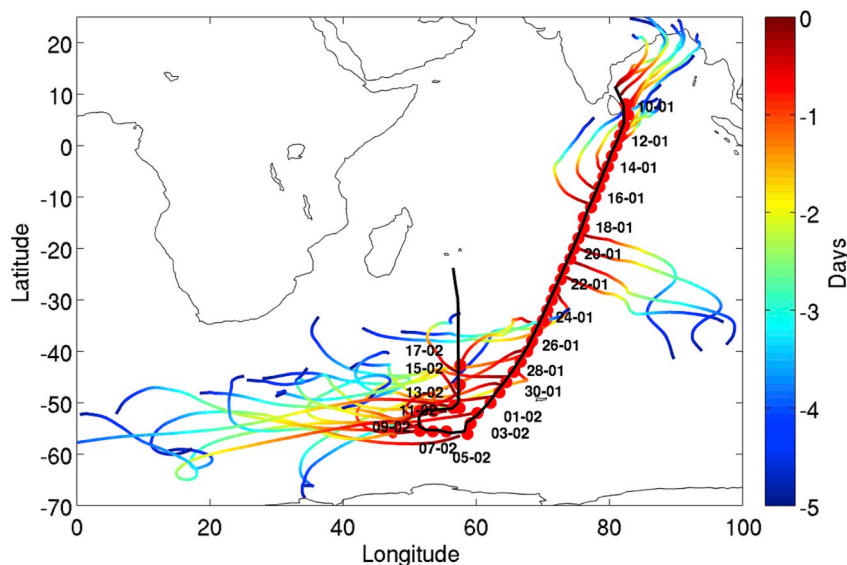

Fig. 1. Cruise track along with the HYSPLIT calculated 5-day back trajectories arriving at locations along the cruise track. The 42 water biogeochemistry sampling stations are marked in red circles.
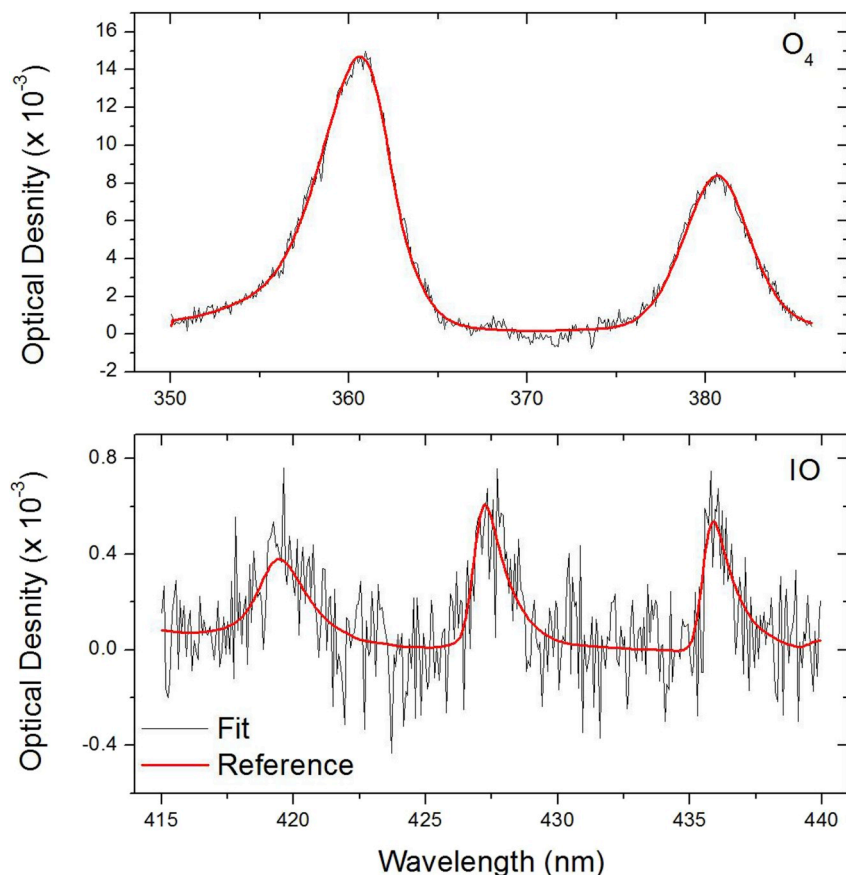
Fig. 2. An example of a DOAS fits for IO and O_4 during the cruise. Both the fits are from 15th January at solar zenith angle (SZA) 44.45° for the 2° elevation. The O_4 DSCD retrieved was $3.3 \times 10^{4^3} \pm 0.2 \times 10^{43}$ molecule^2 cm^{-5}. The RMS was 3.4×10^{-4}. The IO DSCD retrieved was $2.32 \times 10^{13} \pm 1.63 \times 10^{13}$ molecule cm^{-2}. The RMS was 1.62×10^{-4}.

radiative transfer model (Hay et al., 2012) using different aerosol profiles determined by forward modelling. Further details are given in our past work (Gómez Martín et al., 2013; Mahajan et al., 2012; Prados-Roman et al., 2015). IO mixing ratios were then calculated by dividing trace gas DSCDs by the computed path lengths.

2.2. Oceanic observations

Surface chlorophyll *a* (Chl a) was estimated by filtering 4 L of water through GF/F Whatman filter (47 mm), at each station along the transect and the filters were kept frozen (-40 °C) prior to analyses. For total Chl a by fluorometry, the frozen samples were placed in 15 ml
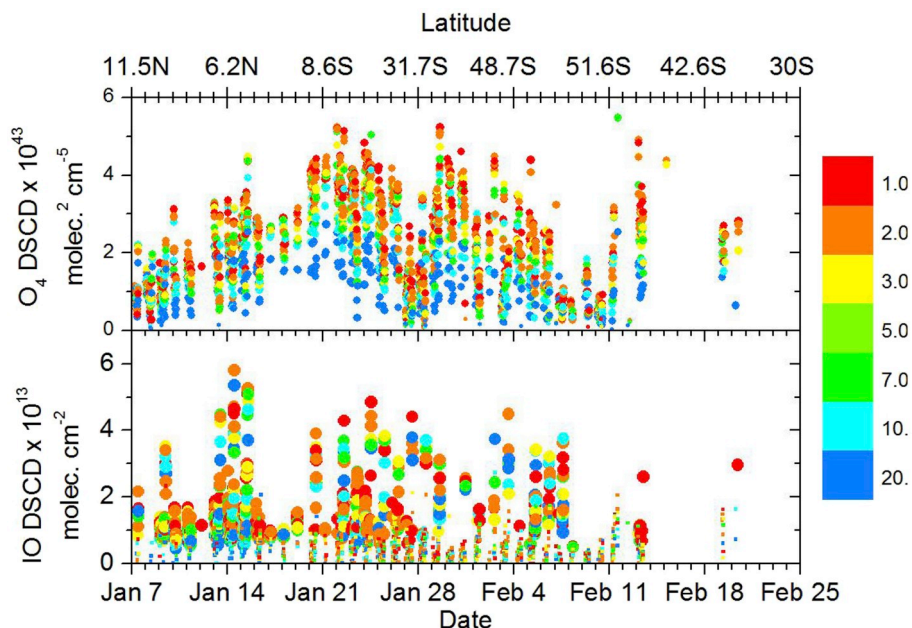

Fig. 3. O_4 and IO DSCDs observed during the cruise. The corresponding latitudes for the dates are shown on the top. The small circles are values below the 2σ detection limit while the larger circles are values above the detection limit.

centrifuge tubes and extracted over night at 4 °C in 10 ml 90% acetone. The extracted samples were measured fluorometrically using Turner's AU10 Fluorometer (Turner Designs Inc.,USA) as described by (Parsons et al., 1984). Calibration was carried out using standard Chl *a* pigments (DHI, Denmark). A Thermosalinograph (SBE21, Sea-Bird electronics, USA) was used to measure the near surface (∼4 m) temperature and salinity, with a sampling period of 10 s. The accuracy for the measurements was temperature: ± 0.001 °C; conductivity: ± 0.0001 S m^{-1}. Additional surface seawater measurements of biogeochemical parameters were carried out at 42 stations along the cruise track (Fig. 1). Samples for nutrient analysis were collected in 250 mL narrow mouth polypropylene amber bottles (Nalgene). Each bottle was rinsed twice with the sample water prior to collection. Analysis was performed as soon as possible using an onboard SKALAR SAN + segmented continuous flow autoanalyser. Although various biogeochemical parameters were measured, we focus on the nitrate due to its strong correlation with the distribution of iodide in the global seawater (Chance et al., 2014). The precision and accuracy for NO_3^- measurements were ± 0.06 and ± 0.07 μM, respectively. For computation of the iodide concentrations along the transect, the observed SST, salinity, nitrate concentrations were used along with the climatological Mixed Layer Depth (MLD_{pt}) from World Ocean Atlas based on the potential temperature difference criteria (0.5 °C) (Monterey and Levitus, 1997) according to parameterisations given by (Chance et al., 2014) using a multiple linear regression analysis of global observations of surface iodide concentrations in the seawater against different parameters:

$$[\text{iodide}] = 0.28 \,(\pm 0.002 \times SST^2 + 1.7(\pm 0.2) \times |\text{latitude}| + 0.9(\pm 0.4) \times [NO_3^-] - 0.020(\pm 0.002) \times MLD_{pt} + 7(\pm 2) \times \text{salinity} - 309(\pm 75) \tag{1}$$

$$\ln[\text{iodide}] = 0.0026(\pm 0.0003) \times SST^2 + 0.016(\pm 0.003) \times |\text{latitude}| - 0.009(\pm 0.006) \times [NO_3^-] - 0.00044(\pm 0.00004) \times MLD_{pt} + 0.05(\pm 0.03) \times \text{salinity} + 2(\pm 1) \tag{2}$$

The obtained parameterisation (Eqs (1) and (2)) showed significant correlations between iodide (nmol L^{-1}) seawater concentration and SST (°C), latitude, MLD_{pt} (in m), nitrate concentration (μmol L^{-1}) and salinity (PSU) with R^2 of respectively 0.676 and 0.642 for the global datasets. Iodide surface concentrations did not show a significant correlation with Chl *a* (< 5% significance level). Iodide concentrations along the cruise track were predicted using both parameterisations (Eq. (1)), and (Eq. (2)), as shown Fig. 4. Consequently the fluxes for I_2 and HOI could be calculated using the predicted iodide seawater concentrations and the parameterisation (Eqs (3) and (4)) proposed by Carpenter et al. (2013) expressions:

$$flux_{I_2} = [O_{3(g)}] * [I^-_{(aq)}]^{1.3} * (1.74 \times 10^9 - 6.54 \times 10^8 * \ln(ws)) \tag{3}$$

$$flux_{HOI} = [O_{3(g)}] * \left(4.15 \times 10^5 * \frac{\sqrt{[I^-_{(aq)}]}}{ws} - \frac{20.6}{ws} - 2.36 \times 10^4 * \sqrt{[I^-_{(aq)}]} \right) \tag{4}$$

where the fluxes are in nmol m^{-2} d^{-1}, [O$_3$] in nmol mol^{-1}, [I$^-$] in mol dm^{-3} and the windspeed (ws) in m s^{-1}. The concentrations using Eq (2) resulted in unrealistically high concentrations of iodide (Fig. 4), particularly at the lower latitudes and overestimates the concentrations of iodide according to very recent observations in this area, however the values using Eq (1) show a good correlation (Tinel et al., manuscript in preparation). Therefore, we consider only the fluxes calculated using Eq (1) for further discussion, although the fluxes using both equations are given for comparison in Fig. 6. The flux for I_2 is particularly affected using Eq (2) which results in very high iodine fluxes, as Eq (3) is more sensitive to the concentration of iodide than Eq (4). During this study, the high wind speeds encountered during the periods of 25–30 January

and 01–06 February led to negative fluxes for I_2, as the last term in the parameterisation becomes negative for wind speed higher than 14.5 m s^{-1}. The proposed parametrisation of the I_2 flux thus seems to be only valid for wind speeds up to 14.5 m s^{-1} as no reasonable physical explanation could explain negative fluxes at high wind speed.

2.3. Modelling

We also make use of the Community Atmospheric Model with Chemistry (CAM-Chem, version 4.0), including a complete chemistry scheme to simulate trace gases and aerosols in the troposphere during the cruise period (Lamarque et al., 2012). A state-of-the-art halogen chemistry scheme (Saiz-Lopez and Fernandez, 2016) has been implemented, including photochemical breakdown of five very short-lived bromocarbons ($CHBr_3$, CH_2Br_2, CH_2BrCl, $CHBrCl_2$, $CHBr_2Cl$) and four iodocarbons (CH_3I, CH_2ICl, CH_2IBr, CH_2I_2) naturally emitted from the ocean (Ordóñez et al., 2012) and inorganic oceanic sources of HOI and I_2 (Carpenter et al., 2013; MacDonald et al., 2014). The simulations were performed in specified dynamic mode (Lamarque et al., 2012), with a spatial resolution of 1.9° latitude by 2.5° longitude and 26 vertical levels, from the surface to ∼40 km (Saiz-Lopez and Fernandez, 2016).

3. Results and discussion

3.1. Meteorology and ozone

Fig. 5 shows the data time series of the meteorological parameters and ozone mixing ratios over the length of the study. The air temperature ranged between 30 °C and 1 °C, with lower temperatures at higher latitudes. The relative humidity (RH) ranged between 50 and 100% over the study. Generally, the air was saturated at colder temperatures in the Southern Ocean. The wind speed ranged between near stagnant conditions at 1 m s^{-1} to about 20 m s^{-1}. Although high wind speeds were observed, rainfall was observed only once during the study on the 16th of January (10.5 °S). The ozone mixing ratios show a distinct reduction in the open ocean environment as compared to the coastal area near the Indian subcontinent. Unfortunately, instrumental problems meant that O$_3$ observations were not possible between 11th January and 19th January. However, levels of about 50 ppbv were observed only close to the Indian subcontinent, with open ocean values ranging between 5 and 20 ppbv. Here, ozone diurnal variation followed a photochemical production regime, peaking during the daytime, while in the open ocean it was variable, with several days showing a decrease during the daytime suggesting photochemical destruction (Fig. 5). The back trajectories also show that continental air masses were sampled until about 15th January (5° N) after which the air masses were not exposed to continental emissions for at least 5 days. Continental air masses are expected to have higher ozone, as observed, due to anthropogenic emissions.

3.2. Iodine chemistry

IO was observed above the detection limit on several days of the cruise (Fig. 3). A peak of 5.8×10^{13} molecules cm^{-2} was observed on 14 January 2015 (6.2° N) corresponding to 0.57 ± 0.27 pptv but the highest mixing ratio of 2.9 ± 1.0 pptv was observed on 7th February (55.6° S) in the Southern Ocean MBL. Larger IO and O$_4$ DSCDs were observed in the lower elevation angles, suggesting that IO showed a decreasing vertical gradient. Decreasing gradients have been observed in the MBL before and are explained by inorganic iodine sources from the surface of the ocean (Gómez Martín et al., 2013; Großmann et al., 2013; Mahajan et al., 2012; Prados-Roman et al., 2015). It should however be noted that detailed vertical gradients were not retrieved during this study and hence it is not possible to compare the vertical profiles with previous works. We hope to explore the vertical profiles of
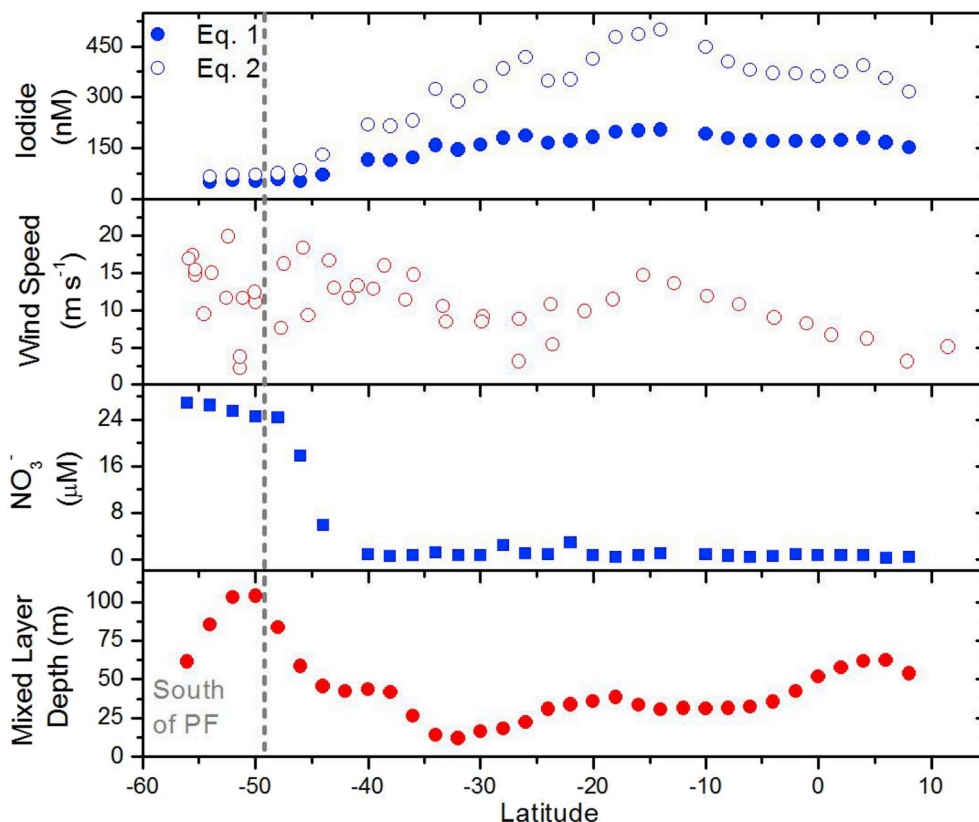
Fig. 4. Latitudinal distribution of iodide, wind speed, NO_3 and MLD values along the latitudinal transect of the cruise calculated using the two parametrisations given in equation (1) (empty circles) and equation (2) (filled circles).

IO and other trace gases in a future work and focus only on the boundary layer concentrations here. The daily averaged IO mixing ratios plotted along the latitudinal transect are shown in Fig. 6. Through most of the study period the daily averaged IO mixing ratios ranged below 0.6 pptv and fell below the detection limit on two days close to the Indian subcontinent. The low values close to the Indian subcontinent are probably due to the titration of IO to below the detection limit by anthropogenic NO_2 to form $IONO_2$. Further along the cruise track, a small increase in the mixing ratios of IO was observed around 40° S followed by a larger increase below 49° S. These areas correspond to the different oceanic fronts, the merged Agulhas Retroflection Front (ARF) and Southern Subtropical Front (SSTF) and the transition between Sub Antarctic Front and the Polar Front (called PF from here on) respectively as indicated by the SST and salinity of Fig. 6. The identification of the fronts was carried out according to the criteria proposed by Holiday and Read (1998). Past observations show that in the Indian sector of the Southern Ocean, the ARF and SSTF are merged as a single front (Anilkumar et al., 2014). Although the highest mixing ratios for IO were observed south of the PF, the IO mixing ratios showed some variability in this area, with the daily averaged values ranging between 0.2 pptv to the highest value of 1.67 ± 0.25 pptv observed on 31st January (~50° S). Higher average mixing ratios (> 0.7 pptv) were observed when the back trajectories came from the sea ice region in Antarctica (e.g. 31st January, 1st February; latitude > 50° S), whereas lower levels < 0.3 pptv were seen when the air masses had only remote oceanic origin, with no exposure to sea ice and had spent little time over the Southern Ocean (e.g. 2nd February, 4th February, > 50° S). Moderate levels are observed when the air mass had spent most of the time in the Southern Ocean, but not exposed to the coastal Antarctic region (e.g. 5th, 6th and 8th of February, > 50° S). The 7th February (55.6°S) is an exception to the observed general pattern of higher IO levels linked to sea ice exposure, when the daily averaged IO elevated at

1.48 ± 0.43 pptv but the air mass not passing over the sea ice region. The reason for this increase is not clear, although it should be mentioned that 7th January (11.5° S) was a sunny day after three days of overcast weather and had relatively lower wind speed, which could play a role in the increased IO levels. It can be speculated that the precursors build up in the air mass due to low photolysis and an subsequent increase in photolysis leads to the release of I atoms and formation of IO. Sea ice has been linked to emissions of iodine compounds in previous studies, which could explain the higher levels in air masses passing close to Antarctica (Atkinson et al., 2012; Saiz-Lopez et al., 2007b). Higher IO has also been observed using satellite data in the Antarctic region (Saiz-Lopez et al., 2007a; Schönhardt et al., 2012, 2008). The process of release of these compounds is still not clear, although the transfer of biologically concentrated iodine through brine channels or cracks has been hypothesized (Saiz-Lopez et al., 2015b).

As mentioned, atmospheric IO concentrations can be driven by the release of inorganic iodine species from the ocean. Fig. 4 shows the computed seawater iodide concentrations and Fig. 6 shows the computed HOI and I_2 fluxes. The fluxes show a strong latitudinal gradient with peak values of 30×10^6 molecules $cm^{-2}\,s^{-1}$ for I_2 and 15×10^8 molecules $cm^{-2}\,s^{-1}$ for HOI close to the Indian subcontinent and a reduction from the northern to the southern hemisphere. The lowest fluxes, 0.5×10^6 molecules $cm^{-2}\,s^{-1}$ for I_2 and 3×10^8 molecules $cm^{-2}\,s^{-1}$ for HOI, are observed in the Southern Ocean, south of the PF. This gradient is mainly driven by ozone, SST and salinity, as explained in detail in section 2.2. According to recent laboratory and modelling studies, the main source of iodine in the MBL is considered to be I_2 and HOI (Carpenter et al., 2013; MacDonald et al., 2014). However, the current study indicates that HOI and I_2 fluxes are poor markers for IO distribution in the Indian Ocean, especially in the Southern Indian Ocean, where the IO concentrations show a peak but the calculated HOI and I_2 fluxes are at their minimum. Considering the low levels of NO_x,
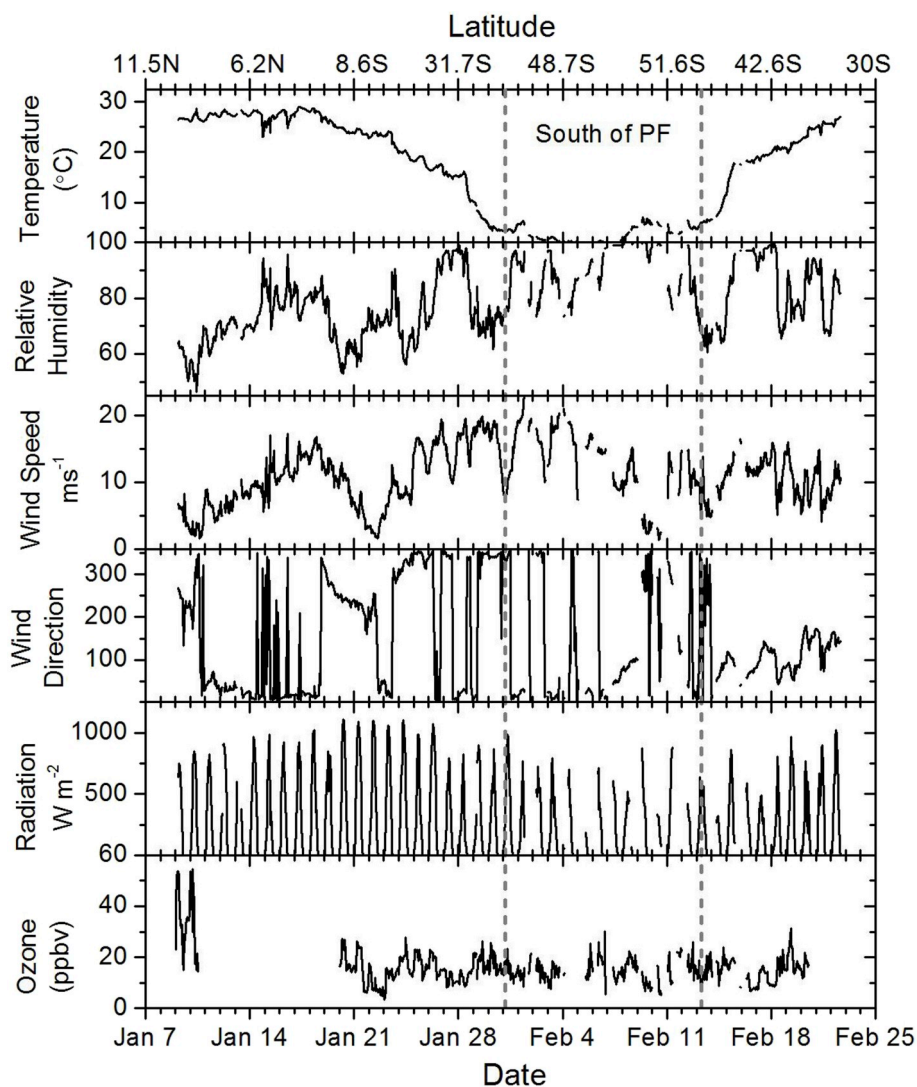
Fig. 5. Data time series of the meteorological parameters and O_3 observed during the cruise. The corresponding latitudes for the dates are given on the top of the plot.

this mismatch is mostly due to other sources playing a dominant role. A possible major source could thus be the emission of iodide compounds from the sea ice region close to Antarctica, which could be of both organic and inorganic origin. These inorganic sources are based three recent suggested mechanisms: i) release of iodine through the equilibrium HOI + I-⇔I$_2$+H$_2$O from sea-ice algae and subsequent diffusion through brine channels to accumulate in the brine layer (Saiz-Lopez et al., 2015a), ii) photolysis of iodate frozen salts (Gálvez et al., 2016), and iii) emission of gaseous iodine from the production of triiodide (I$_3^-$) via iodide oxidation in frozen solution (Kim et al., 2016). The reaction of HOI with dissolved organic matter in the sea ice and snowpack can then form the iodine organic species (Carpenter et al., 2005). It should also be remembered that we use a proxy for the seawater iodide concentrations, although recent observations show the proxy to be fairly accurate in the region under consideration (unpublished data). The calculation of the iodine compound fluxes depends on the seawater iodide and has been estimated through laboratory experiments (Carpenter et al., 2013), and has also been validated through other field observations (MacDonald et al., 2014). It is currently the latest estimation available and is used in most models (Prados-Roman et al., 2015; Saiz-Lopez et al., 2014; Sherwen et al., 2016a), but further direct estimation of fluxes is encouraged.

The increase in IO mixing ratios observed on 27th and 28th January (0.94 ± 0.42 pptv and 0.55 ± 0.28 pptv close to 40° S) is also not driven by sea ice emissions, as indicated by the back trajectories (Fig. 1). However, the chl *a* values on these two days were the highest observed during the cruise (~0.9 μg L^{-1}) as this frontal oceanic region is dynamically unstable due to the presence of the Agulhas return current. This results in the merged ARF and SSTF to be characterised by high mesoscale turbulence causing intermittent phytoplankton blooms in this region (Llido et al., 2005). Correlations between chl *a* and iodine species have been reported in previous studies and can be particularly strong for organic and particulate iodine in highly productive regions, such as the Atlantic Ocean off-coast to Argentina (Lai et al., 2011), although poor correlations were observed in the Eastern Atlantic Ocean. However, direct correlations between chl *a* and IO seem less straightforward (Großmann et al., 2013; Mahajan et al., 2012). Phytoplankton has been implicated in the production of very short lived organoiodides (CH$_3$I, C$_2$H$_5$I, CH2I$_2$, CH$_2$IBr, CH$_2$ICl etc.), which are precursors to IO (Moore and Groszko, 1999). Indeed, in coastal environments macroaglae are have been shown to be a significant source (Carpenter, 2003; Carpenter et al., 2003). In the open ocean environment in the Atlantic Ocean and Southern Ocean, a poor correlation between emissions of organoiodides and chl *a* has been reported (Chuck et al., 2005). Observations at the Cape Verde Atmospheric Laboratory, and along a cruise in the tropical east Atlantic Ocean showed significant sea-air fluxes for organoiodides (Jones et al., 2010). One dimensional model simulations predicted that these fluxes could result in ~0.45
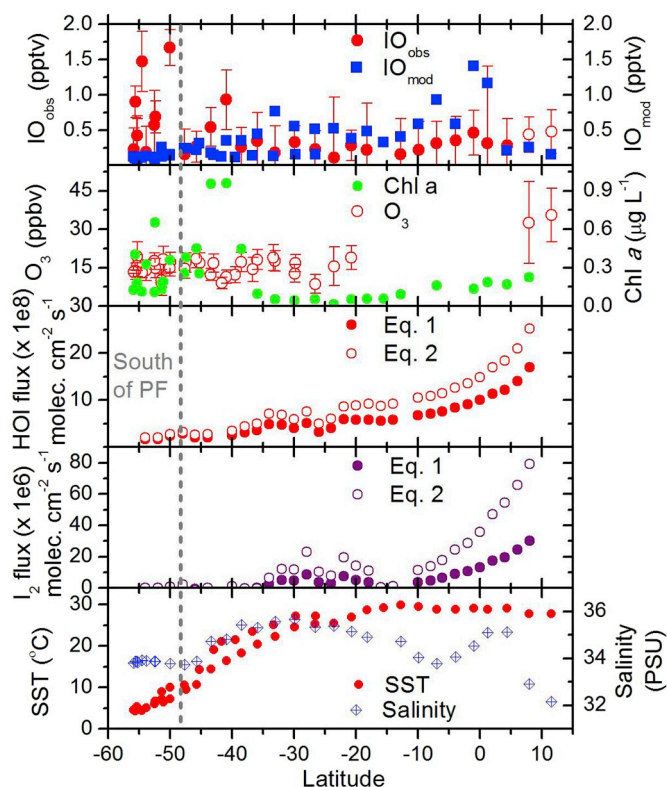
Fig. 6. Daily averaged values of oceanic and atmospheric parameters observed during the cruise. The calculated HOI and I_2 ocean-air fluxes according to the parameterisation given by (Chance et al., 2014) are shown. The empty circles represent the fluxes calculated using equation (1) and the filled circles show the values calculated using equation (2). The first panel also shows the modelled IO, simulated using the model CAM-Chem.

pptv of IO in the MBL (Mahajan et al., 2010), which is in the same range of mixing ratios that were observed during the current study. This suggests that it is possible for organic iodine emissions to play a significant role in the Indian Ocean MBL. However, global models suggest that the inorganic sources contribute about 75% of the boundary layer iodine loading (Prados-Roman et al., 2015). Therefore, we study the correlations between IO and various oceanic and atmospheric parameters (Fig. 7) in order to understand the drivers behind atmospheric IO.

These parameters (O_3, chl a, SST, salinity, wind speed, seawater iodide concentration, I_2 and HOI fluxes) are chosen because they are considered to be strong drivers for iodine emissions (Carpenter et al., 2013). In the past, observations in the Eastern Pacific have shown that IO is positively correlated to SST and salinity, but negatively to the atmospheric O_3 and chl a (> 99% confidence), while the correlation with wind speed was not statistically significant (Mahajan et al., 2012). Observations in the western Pacific have shown similar results, with the exception of chl a which showed a poor correlation with IO in that region (Großmann et al., 2013). However, during this study we find that none of the parameters are positively correlated at 99% confidence with IO (Fig. 7). Indeed, only chl a is correlated above the 90% confidence limit, with a positive R value of 0.34 (P = 0.08, n = 30), unlike in the Eastern Pacific. IO is negatively correlated with SST (R = −0.44, P = 0.16, n = 30), which is contrary to previous reports (Großmann et al., 2013; Mahajan et al., 2012). The seawater iodide concentrations are negatively correlated to atmospheric IO (R = −0.46, P = 0.02), while the HOI and I_2 fluxes do not show a significant correlation. This is surprising considering that the current state-of-the-art assumes ozone deposition driven I_2 and HOI to be the main sources of iodine in the atmosphere (Carpenter et al., 2013).

If we only consider the observations only north of the PF, the correlation coefficient between chl a and IO is significant at 99% (R = 0.75, P = 0.0003, n = 21; Fig. 8). The correlations with other oceanic parameters for this subset are not significant. Past studies from the Pacific have found chl a to be a poor proxy for iodine (Großmann et al., 2013; Mahajan et al., 2012), but the strong correlation between
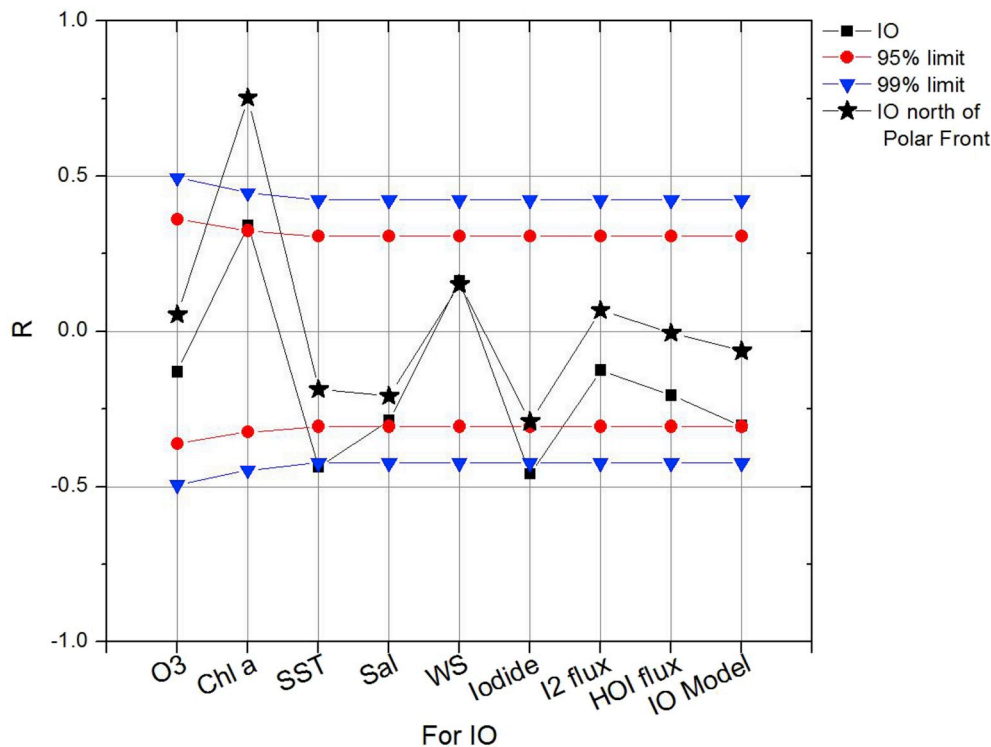

Fig. 7. Correlation coefficients of IO with other observed parameters, along with 95% and 99% confidence limits are shown. The squares are the correlation coefficients when the whole dataset is included (n = 30) and the stars indicates the correlation coefficient when only the observations north of the polar front are considered (n = 21).
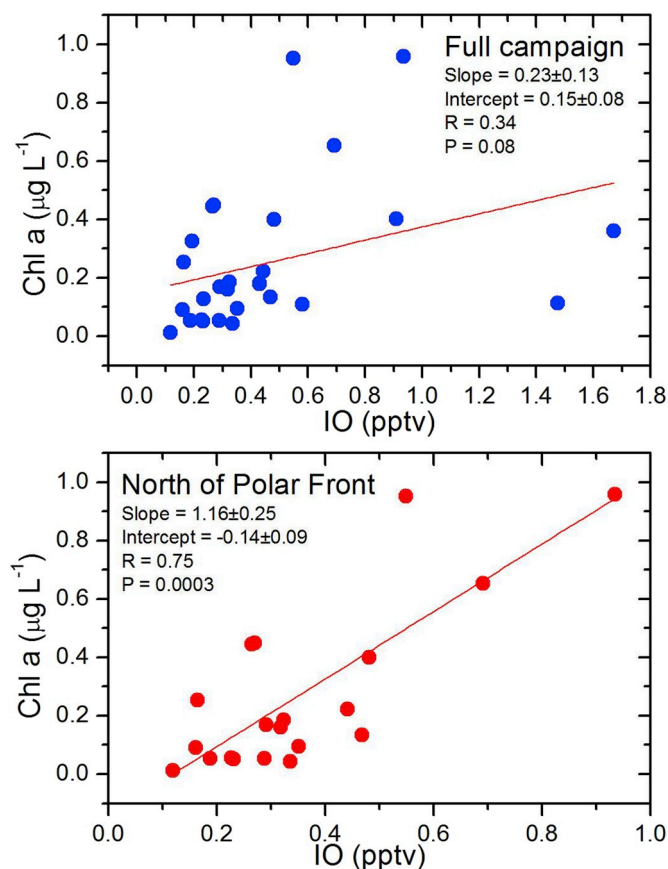
Fig. 8. Linear fit of IO with chl *a* for the full study and for measurements above the Polar Front. The respective Pearsons correlation coefficient along with the P value is also given.

IO and chl *a*, suggest that phytoplankton distribution is a better proxy for atmospheric IO in the Indian Ocean, especially above the PF (Fig. 8). Although this relationship has not been observed on a global level, it has been suggested that a strong connection between organic iodine species, particulate iodine and the phytoplankton in the ocean exists in the Southern Atlantic Ocean (Lai et al., 2011). The current results also show that although HOI and I_2 are the main fluxes of iodine into the atmosphere in the other oceans (Carpenter et al., 2013; MacDonald et al., 2014), and chl *a* is a poor proxy for iodide in the seawater (Chance et al., 2014), chl *a* cannot be dismissed as a proxy for atmospheric IO in the remote environment of the Indian Ocean.

Finally, we compare the observations with simulations from CAM-Chem, which has recently been used to study global halogen chemistry (Ordóñez et al., 2012; Prados-Roman et al., 2015; Saiz-Lopez et al., 2012). A comparison of the daily averaged surface IO fields between 0600 and 1800 h simulated by the model and observations has been done before, although there were very few observations available in the Indian Ocean and none in the Southern Ocean (Prados-Roman et al., 2015). Fig. 6 shows the comparison between the modelled and observed IO. The model shows elevated IO close to the Equator, while in most other locations it is less than 0.5 pptv. According to the model, higher concentrations are expected in the tropics and extra tropics (Prados-Roman et al., 2015). The gradient is driven by the emission strength of inorganic source gases (HOI/I_2), which are in turn driven by the rate of ozone deposition and the iodide content in the seawater (Carpenter et al., 2013; MacDonald et al., 2014), which is para-meterized to the SST, leading to a peak around the Equator. Although the model does replicate absolute levels of IO for most of the cruise, it fails to capture the increase south of the PF. The correlation between the model and observed IO is negative and not highly significant

($R = -0.30$, $P = 0.10$, $n = 30$; Fig. 7). It should be noted that the model currently does not include any sea ice and snowpack emissions for iodine, which could contribute to the mismatch between the observations and the model, especially south of the PF. These observations show the need to include sea-ice emissions for iodine compounds to improve the model-observations match over the Southern Ocean. If we consider only the observations north of the PF, the correlation coefficient is still not significant ($R = -0.06$, $P = 0.79$, $n = 30$; Fig. 7). The observations also do not see a distinct increase in IO mixing ratios close to the Equator. The main reason for this mismatch is the indirect parameterisation of the emissions of iodine compounds with SST, which is a poor driver for atmospheric IO in the Indian Ocean according to the current observations. This suggests that the emissions of iodine compounds are more complex than considered hitherto and that further work on the estimation of fluxes in the field is necessary to achieve a better match between the model and the observations.

4. Conclusions

Observations of IO and O3 were made on a 45 day long cruise in the Indian Ocean. This is the first time such a transect of atmospheric trace gas measurements was made in this region. IO was detected during the study, and showed an increase south of the PF. IO shows a positive correlation with chl *a* and a negative correlation with SST, contrary to previous observations in the Pacific Ocean. Comparison with model simulations show that in locations with elevated chl *a*, there is a poor match with the model, which suggests that organic iodine precursors could contribute towards reactive iodine in the region studied. The results indicate that we do not completely understand the sources of iodine in the MBL, especially in the remote Southern Ocean MBL. There is a need for laboratory experiments and field studies to enable more accurate parameterisations for the emissions of reactive iodine compounds from the sea surface.

Conflicts of interest

We confirm that the authors do not have any conflict of interest.

References

Alicke, B., Hebestreit, K., Stutz, J., Platt, U., 1999. Iodine oxide in the marine boundary layer. Nature 397, 572–573. https://doi.org/10.1038/17508.

Allan, B., McFiggans, G., Plane, J.M.C., Coe, H., 2000. Observations of iodine monoxide in the remote marine boundary layer. J. Geophys. 105, 14363–14369.

Anilkumar, N., George, J.V., Chacko, R., Nuncio, N., Sabu, P., 2014. Variability of fronts, fresh water input and chlorophyll in the Indian Ocean sector of the Southern Ocean. N. Z. J. Mar. Freshw. Res. https://doi.org/10.1080/00288330.2014.924972.

Atkinson, H.M., Huang, R.-J., Chance, R., Roscoe, H.K., Hughes, C., Davison, B., Schönhardt, A., Mahajan, A.S., Saiz-Lopez, A., Hoffmann, T., Liss, P.S., 2012. Iodine emissions from the sea ice of the Weddell Sea. Atmos. Chem. Phys. 12, 11229–11244. https://doi.org/10.5194/acp-12-11229-2012.

Bogumil, K., Orphal, J., Homann, T., Voigt, S., Spietz, P., Fleischmann, O.C., Vogel, A., Hartmann, M., Kromminga, H., Bovensmann, H., Frerick, J., Burrows, J.P., 2003. Measurements of molecular absorption spectra with the SCIAMACHY pre-flight model: instrument characterization and reference data for atmospheric remote-sensing in the 230–2380 nm region. J. Photochem. Photobiol. Chem. 157, 167–184. https://doi.org/10.1016/S1010-6030(03)00062-5.

Carpenter, L.J., 2003. Iodine in the marine boundary layer. Chem. Rev. 103, 4953–4962. https://doi.org/Doi.10.1021/Cr0206465.

Carpenter, L.J., Hoppkins, J.B., Jones, C.E., Lewis, A.C., Parthipan, R., Wevill, D.J., 2005. Abiotic source of reactive organic halogens in the sub-arctic atmosphere? Environ. Sci. Technol. 39, 8812–8816.

Carpenter, L.J., Liss, P.S., Penkett, S.A., 2003. Marine organohalogens in the atmosphere over the atlantic and southern oceans. J. Geophys. Res. 108. https://doi.org/10.1029/2002JD002769.

Carpenter, L.J., MacDonald, S.M., Shaw, M.D., Kumar, R., Saunders, R.W., Parthipan, R., Wilson, J., Plane, J.M.C., 2013. Atmospheric iodine levels influenced by sea surface emissions of inorganic iodine. Nat. Geosci. 6, 108–111. https://doi.org/10.1038/ngeo1687.

Chance, R., Baker, A.R., Carpenter, L., Jickells, T.D., 2014. The distribution of iodide at the sea surface. Environ. Sci. Process. Impacts. https://doi.org/10.1039/c4em00139g.

Chance, K.V., Spurr, R.J., 1997. Ring effect studies: Rayleigh scattering, including molecular parameters for rotational Raman scattering, and the Fraunhofer spectrum. Appl. Opt. 36, 5224–5230.

Chuck, A.L., Turner, S.M., Liss, P.S., 2005. Oceanic distributions and air-sea fluxes of biogenic halocarbons in the open ocean. J. Geophys. Res. 110. https://doi.org/10.1029/2004JC002741.

Coburn, S., Dix, B., Sinreich, R., Volkamer, R., 2011. The CU ground MAX-DOAS instrument: characterization of RMS noise limitations and first measurements near Pensacola, FL of BrO, IO, and CHOCHO. Atmos. Meas. Tech. 4, 2421–2439. https://doi.org/10.5194/amt-4-2421-2011.

Commane, R., Seitz, K., Bale, C.S.E., Bloss, W.J., Buxmann, J., Ingham, T., Platt, U., Pöhler, D., Heard, D.E., 2011. Iodine monoxide at a clean marine coastal site: observations of high frequency variations and inhomogeneous distributions. Atmos. Chem. Phys. 11, 6721–6733. https://doi.org/10.5194/acp-11-6721-2011.

Dix, B., Baidar, S., Bresch, J.F., Hall, S.R., Schmidt, K.S., Wang, S., Volkamer, R., 2013. Detection of iodine monoxide in the tropical free troposphere. Proc. Natl. Acad. Sci. U.S.A. 110, 2035–2040. https://doi.org/10.1073/pnas.1212386110.

Draxler, R., Rolph, G., 2003. HYSPLIT (HYbrid single particle Lagrangian integrated trajectory). Model access via NOAA ARL Ready [WWW Document]. URL. http://www.arl.noaa.gov/ready/hysplit4.html.

Fayt, C., Van Roozendael, M., 2013. QDOAS 1.00. Software User Manual [WWW Document]. URL. http://uv-vis.aeronomie.be/software/QDOAS/.

Frieß, U., Wagner, T., Pundt, I., Pfeilsticker, K., Platt, U., Friefi, U., 2001. Spectroscopic measurements of tropospheric iodine oxide at neumayer station, Antarctica. Geophys. Res. Lett. 28, 1941–1944.

Gálvez, Ó., Teresa Baeza-Romero, M., Sanz, M., Saiz-Lopez, A., 2016. Photolysis of frozen iodate salts as a source of active iodine in the polar environment. Atmos. Chem. Phys. 16, 12703–12713. https://doi.org/10.5194/acp-16-12703-2016.

Gómez Martín, J.C., Mahajan, A.S., Hay, T.D., Prados-Román, C., Ordóñez, C., MacDonald, S.M., Plane, J.M.C., Sorribas, M., Gil, M., Mora, J.F.P., Reyes, M.V.A., Oram, D.E., Leedham, E., Saiz-Lopez, A., 2013. Iodine chemistry in the eastern Pacific marine boundary layer. J. Geophys. Res. Atmos. 118, 1–18. https://doi.org/10.1002/jgrd.50132.

Gómez Martín, J.C., Spietz, P., Burrows, J.P., 2005. Spectroscopic studies of the I-2/O-3 photochemistry - Part 1: determination of the absolute absorption cross sections of iodine oxides of atmospheric relevance. J. Photochem. Photobiol. Chem. 176, 15–38. https://doi.org/10.1016/j.jphotochem.2005.09.024.

Greenblatt, G.D., Orlando, J.J., Burkholder, J.B., Ravishankara, A.R., 1990. Absorption measurements of oxygen between 330 and 1140 nm. J. Geophys. Res. 95, 18577–18582.

Großmann, K., Frieß, U., Peters, E., Wittrock, F., Lampel, J., Yilmaz, S., Tschritter, J., Sommariva, R., von Glasow, R., Quack, B., Krüger, K., Pfeilsticker, K., Platt, U., 2013. Iodine monoxide in the Western Pacific marine boundary layer. Atmos. Chem. Phys. 13, 3363–3378. https://doi.org/10.5194/acp-13-3363-2013.

Hausmann, M., Platt, U., 1994. Spectroscopic measurement of bromine oxide and ozone in the high arctic during polar sunrise experiment 1992. J. Geophys. Res. Atmos. 99, 25399–25413.

Hay, T.D., Bodeker, G.E., Kreher, K., Schofield, R., B, L., Scherer, M., McDonald, A.J., 2012. The NIMO Monte Carlo radiative transfer model for box-air-mass-factor and radiance calculations. J. Quant. Spectrosc. Radiat. Transf. 113, 721–738. https://doi.org/10.1016/j.jqsrt.2012.02.005.

Holiday, N.P., Read, J.F., 1998. Surface oceanic fronts between Africa and Antarctica. Deep-Sea Res. Part I Oceanogr. Res. Pap. 45, 217–218.

Hönninger, G., von Friedeburg, C., Platt, U., 2003. Multi Axis di ff erential optical absorption spectroscopy (MAX-DOAS). Atmos. Chem. Phys. Discuss. 3, 5595–5658.

Jones, C.E., Hornsby, K.E., Sommariva, R., Dunk, R.M., Von Glasow, R., McFiggans, G., Carpenter, L.J., 2010. Quantifying the contribution of marine organic gases to atmospheric iodine. Geophys. Res. Lett. 37. https://doi.org/10.1029/2010GL043990.

Kim, K., Yabushita, A., Okumura, M., Saiz-Lopez, A., Cuevas, C.A., Blaszczak-Boxe, C.S., Min, D.W., Yoon, H. Il, Choi, W., 2016. Production of molecular iodine and tri-iodide in the frozen solution of iodide: implication for polar atmosphere. Environ. Sci. Technol. 50, 1280–1287. https://doi.org/10.1021/acs.est.5b05148.

Lai, S.C., Williams, J., Arnold, S.R., Atlas, E.L., Gebhardt, S., Hoffmann, T., 2011. Iodine containing species in the remote marine boundary layer: a link to oceanic phytoplankton. Geophys. Res. Lett. 38, 1–5. https://doi.org/10.1029/2011GL049035.

Lamarque, J.-F., Emmons, L.K., Hess, P.G., Kinnison, D.E., Tilmes, S., Vitt, F., Heald, C.L., Holland, E. a., Lauritzen, P.H., Neu, J., Orlando, J.J., Rasch, P.J., Tyndall, G.K., 2012. CAM-chem: description and evaluation of interactive atmospheric chemistry in the community Earth system model. Geosci. Model Dev. (GMD) 5, 369–411. https://doi.org/10.5194/gmd-5-369-2012.

Leser, H., Honninger, G., Platt, U., 2003. MAX-DOAS measurements of BrO and NO2 in the marine boundary layer. Geophys. Res. Lett. 30, 1537.

Llido, J., Garçon, V., Lutjeharms, J.R.E., Sudre, J., 2005. Event-scale blooms drive enhanced primary productivity at the subtropical convergence. Geophys. Res. Lett. 32.

MacDonald, S.M., Gómez Martín, J.C., Chance, R., Warriner, S., Saiz-Lopez, A., Carpenter, L.J., Plane, J.M.C., 2014. A laboratory characterisation of inorganic iodine emissions from the sea surface: dependence on oceanic variables and parameterisation for global modelling. Atmos. Chem. Phys. 14, 5841–5852. https://doi.org/10.5194/acp-14-5841-2014.

Mahajan, A.S., Gómez Martín, J.C., Hay, T.D., Royer, S.-J., Yvon-Lewis, S.A., Liu, Y., Hu, L., Prados-Román, C., Ordóñez, C., Plane, J.M.C., Saiz-Lopez, A., 2012. Latitudinal distribution of reactive iodine in the Eastern Pacific and its link to open ocean sources. Atmos. Chem. Phys. 12, 11609–11617. https://doi.org/10.5194/acp-12-11609-2012.

Mahajan, A.S., Plane, J.M.C., Oetjen, H., Mendes, L.M., Saunders, R.W., Saiz-Lopez, A., Jones, C.E., Carpenter, L.J., McFiggans, G.B., 2010. Measurement and modelling of tropospheric reactive halogen species over the tropical Atlantic Ocean. Atmos. Chem. Phys. 10, 4611–4624.

Martin, M., Pöhler, D., Seitz, K., Sinreich, R., Platt, U., 2009. BrO measurements over the eastern north-atlantic. Atmos. Chem. Phys. 9, 9545–9554.

McConnell, J.C., Henderson, G.S., Barrie, L.A., Bottenheim, J.W., Niki, H., Landford, C.H., Templeton, E.M.J., 1992. Photochemical bromine production implicated in arctic boundary layer ozone depletion. Nature 355, 150–152.

Meller, R., Moortgat, G.K., 2000. Temperature dependence of the absorption cross sections of formaldehyde between 223 and 323 K in the wavelength range 225-375 nm. J. Geophys. Res. 105, 7089–7101.

Monterey, G., Levitus, S., 1997. Seasonal Variability of Mixed Layer Depth for the World Ocean. U.S. Government Printing Office, Washington, D.C.

Moore, R.M., Groszko, W., 1999. Methyl iodide distribution in the ocean and fluxes to the atmosphere. J. Geophys. Res. 104, 11163–11171.

Oetjen, H., 2009. Measurements of Halogen Oxides by Scattered Sunlight Differential Optical Absorption Spectroscopy. University of Bremen.

Ordóñez, C., Lamarque, J.-F., Tilmes, S., Kinnison, D.E., Atlas, E.L., Blake, D.R., Sousa Santos, G., Brasseur, G., Saiz-Lopez, A., 2012. Bromine and iodine chemistry in a global chemistry-climate model: description and evaluation of very short-lived oceanic sources. Atmos. Chem. Phys. 12, 1423–1447. https://doi.org/10.5194/acp-12-1423-2012.

Parsons, T.R., Maita, Y., Lalli, C.M., 1984. A Manual of Chemical and Biological Methods for Seawater Analysis. Pergamon Press, Oxford.

Plane, J.M.C., Saiz-Lopez, A., 2006. UV-visible differential optical absorption spectroscopy (DOAS). In: Heard, D.E. (Ed.), Analytical Techniques for Atmospheric Measurement. Wiley-Blackwell, pp. 147–188.

Platt, U., Stutz, J., 2008. Differential Optical Absorption Spectroscopy: Principles and Applications, first ed. ed. Springer.

Pope, R.M., Fry, E.S., 1997. Absorption spectrum (380–700 nm) ofpure water . II . Integrating cavity measurements. Appl. Opt. 36, 8710–8723.

Prados-Roman, C., Cuevas, C. a., Hay, T., Fernandez, R.P., Mahajan, A.S., Royer, S.-J., Galí, M., Simó, R., Dachs, J., Großmann, K., Kinnison, D.E., Lamarque, J.-F., Saiz-Lopez, A., 2015. Iodine oxide in the global marine boundary layer. Atmos. Chem. Phys. 15, 583–593. https://doi.org/10.5194/acp-15-583-2015.

Read, K.A., Mahajan, A.S., Carpenter, L.J., Evans, M.J., Faria, B.V.E., Heard, D.E., Hopkins, J.R., Lee, J.D., Moller, S.J., Lewis, A.C., Mendes, L.M., McQuaid, J.B., Oetjen, H., Saiz-Lopez, A., Pilling, M.J., Plane, J.M.C., 2008. Extensive halogen-mediated ozone destruction over the tropical Atlantic Ocean. Nature 453, 1232–1235.

Rothman, L.S., Gordon, I.E., Babikov, Y., Barbe, A., Chris Benner, D., Bernath, P.F., Birk, M., Bizzocchi, L., Boudon, V., Brown, L.R., Campargue, A., Chance, K., Cohen, E. a., Coudert, L.H., Devi, V.M., Drouin, B.J., Fayt, A., Flaud, J.-M., Gamache, R.R., Harrison, J.J., Hartmann, J.-M., Hill, C., Hodges, J.T., Jacquemart, D., Jolly, A., Lamouroux, J., Le Roy, R.J., Li, G., Long, D. a., Lyulin, O.M., Mackie, C.J., Massie, S.T., Mikhailenko, S., Müller, H.S.P., Naumenko, O.V., Nikitin, A.V., Orphal, J., Perevalov, V., Perrin, A., Polovtseva, E.R., Richard, C., Smith, M. a. H., Starikova, E., Sung, K., Tashkun, S., Tennyson, J., Toon, G.C., Tyuterev, V.G., Wagner, G., 2013. The HITRAN 2012 molecular spectroscopic database. J. Quant. Spectrosc. Radiat. Transf. 130, 4–50. https://doi.org/10.1016/j.jqsrt.2013.07.002.

Saiz-Lopez, A., Baidar, S., Cuevas, C.A., Koenig, T.K., Fernandez, R.P., Dix, B., Kinnison, D.E., Lamarque, J., Rodriguez-Lloveras, X., Campos, T.L., Volkamer, R., 2015a. Injection of iodine to the stratosphere. Geophys. Res. Lett. 42, 6852–6859. https://doi.org/10.1002/2015GL064796.

Saiz-Lopez, A., Blaszczak-Boxe, C.S., Carpenter, L.J., 2015b. A mechanism for biologically-induced iodine emissions from sea-ice. Atmos. Chem. Phys. 15, 9731–9746. https://doi.org/10.5194/acp-15-9731-2015.

Saiz-Lopez, A., Chance, K.V., Liu, X., Kurosu, T.P., Sander, S.P., 2007a. First observations of iodine oxide from space. Geophys. Res. Lett. 34, L12812. https://doi.org/10.1029/2007GL030111.

Saiz-Lopez, A., Fernandez, R.P., 2016. On the formation of tropical rings of atomic halogens: causes and implications. Geophys. Res. Lett. 43, 1–8. https://doi.org/10.1002/2015GL067608.

Saiz-Lopez, A., Fernandez, R.P., Ordóñez, C., Kinnison, D.E., Gómez Martín, J.C., Lamarque, J.-F., Tilmes, S., 2014. Iodine chemistry in the troposphere and its effect on ozone. Atmos. Chem. Phys. 14, 13119–13143. https://doi.org/10.5194/acp-14-13119-2014.

Saiz-Lopez, A., Lamarque, J.-F., Kinnison, D.E., Tilmes, S., Ordóñez, C., Orlando, J.J., Conley, A.J., Plane, J.M.C., Mahajan, A.S., Sousa Santos, G., Atlas, E.L., Blake, D.R., Sander, S.P., Schauffler, S., Thompson, a. M., Brasseur, G., 2012. Estimating the climate significance of halogen-driven ozone loss in the tropical marine troposphere. Atmos. Chem. Phys. 12, 3939–3949. https://doi.org/10.5194/acp-12-3939-2012.

Saiz-Lopez, A., Mahajan, A.S., Salmon, R.A., Bauguitte, S.J.-B., Jones, A.E., Roscoe, H.K., Plane, J.M.C., 2007b. Boundary layer halogens in coastal Antarctica. Science (80-.) 317, 348–351. https://doi.org/10.1126/science.1141408.

Saiz-Lopez, A., Plane, J.M.C., 2004. Novel iodine chemistry in the marine boundary layer. Geophys. Res. Lett. 31, L04112. https://doi.org/10.1029/2003GL019215.

Saiz-Lopez, A., von Glasow, R., 2012. Reactive halogen chemistry in the troposphere. Chem. Soc. Rev. https://doi.org/10.1039/c2cs35208g.

Schönhardt, a., Begoin, M., Richter, a., Wittrock, F., Kaleschke, L., Gómez Martín, J.C.,

Burrows, J.P., 2012. Simultaneous satellite observations of IO and BrO over Antarctica. Atmos. Chem. Phys. 12, 6565–6580. https://doi.org/10.5194/acp-12-6565-2012.

Schönhardt, A., Richter, A., Wittrock, F., Kirk, H., Oetjen, H., Roscoe, H.K., Burrows, J.P., 2008. Observations of iodine monoxide columns from satellite. Atmos. Chem. Phys. 8, 637–653.

Sherwen, T., Evans, M.J., Carpenter, L.J., Andrews, S.J., Lidster, R.T., Dix, B., Koenig, T.K., Volkamer, R., Saiz-Lopez, A., Prados-Roman, C., Mahajan, A.S., Ordóñez, C., 2016a. Iodine's impact on tropospheric oxidants: a global model study in. GEOS-Chem. Atmos. Chem. Phys. 16, 1161–1186. https://doi.org/10.5194/acp-16-1161-2016.

Sherwen, T., Schmidt, J.A., Evans, M.J., Carpenter, L.J., Großmann, K., Eastham, S.D., Jacob, D.J., Dix, B., Koenig, T.K., Sinreich, R., Ortega, I., Volkamer, R., Saiz-Lopez, A., Prados-Roman, C., Mahajan, A.S., Ordóñez, C., 2016b. Global impacts of tropospheric halogens (Cl, Br, I) on oxidants and composition in GEOS-Chem. Atmos. Chem. Phys. 16, 12239–12271. https://doi.org/10.5194/acp-2016-424.

Sinreich, R., Coburn, S., Dix, B., Volkamer, R., 2010. Ship-based detection of glyoxal over the remote tropical Pacific Ocean. Atmos. Chem. Phys. 10, 11359–11371. https://doi.org/10.5194/acp-10-11359-2010.

Vandaele, A.C., Hermans, C., Simon, P., Carleer, M.R., Colins, R., Fally, F., Merienne, M.F., Jenouvrier, A., Coquart, B., 1997. Measurements of NO2 absorption cross-sections at 42000 cm-1 to 10000 cm-1 (238-1000 nm) at 220 K and 298 K. J. Quant. Spectrosc. Radiat. Transf. 59, 171–184.

Wagner, T., Beirle, S., Deutschmann, T., 2009. Three-dimensional simulation of the Ring effect in observations of scattered sun light using Monte Carlo radiative transfer models. Atmos. Meas. Tech. 2, 113–124. https://doi.org/10.5194/amt-2-113-2009.

Wagner, T., Dix, B., Friedeburg, C.V., Frieß, U., Sanghavi, S., Sinreich, R., Platt, U., 2004. MAX-DOAS O 4 measurements: a new technique to derive information on atmospheric aerosols—principles and information content. J. Geophys. Res. 109. https://doi.org/10.1029/2004JD004904.

Wang, F., Saiz-Lopez, A., Mahajan, A.S., Gómez Martín, J.C., Armstrong, D., Lemes, M., Hay, T., Prados-Roman, C., 2014. Enhanced production of oxidised mercury over the tropical Pacific Ocean: a key missing oxidation pathway. Atmos. Chem. Phys. 14, 1323–1335. https://doi.org/10.5194/acp-14-1323-2014.

Wilmouth, D.M., Hanisco, T.F., Donahue, N.M., Anderson, J.G., 1999. Fourier transform ultraviolet spectroscopy of the A 2Π3/2 ← X 2Π3/2 transition of BrO. J. Phys. Chem. 103, 8935–8945.